Component-Specific Analysis of Plasma Protein Corona Formation on Gold Nanoparticles Using Multiplexed Surface Plasmon Resonance

Abhijeet Patra, Tao Ding, Gokce Engudar, Yi Wang, Michal Marcin Dykas, Bo Liedberg, James Chen Yong Kah,* Thirumalai Venkatesan,* and Chester Lee Drum*

At the nano–bio interface, human plasma differentially interacts with engineered nanomaterials through the creation of protein coronas, which in turn become primary determinants of both the pharmacokinetics and pharmacodynamics of circulating nanoparticles. Here, for the first time, the specific binding kinetics of the four major corona forming proteins (human serum albumin, fibrinogen, ApoA1, and polyclonal IgG) are determined for gold nanoparticles (AuNPs). Using a multiplexed surface plasmonic assay, highly reproducible measurements of on rate (k_{on}), off rate (k_{off}), and disassociation constant (K_D), in addition to relative amounts of protein binding, are obtained. Dramatic differences in k_{on} for individual components are shown as primary determinants of protein affinities, with k_{on} ranging over nearly two orders of magnitude for the proteins studied, while k_{off} remains within a factor of two for the set. The effect of polyethylene glycol (PEG) modification on plasma component binding is also studied and the effect of PEG length on human serum interaction is characterized through systematic screening of PEG molecular weight (2–30k). The effect of nanoparticle modification on particle targeting is also characterized through study of a hybrid AuNP system.

A. Patra, M. M. Dykas, Prof. T. Venkatesan
NUSNNI-NanoCore
National University of Singapore
5A Engineering Drive 1, 11411, Singapore
E-mail: venky@nus.edu.sg

A. Patra, M. M. Dykas, Prof. T. Venkatesan
NUS Graduate School for Integrative Sciences and Engineering
National University of Singapore
28 Medical Drive, 117456, Singapore

Dr. T. Ding, Prof. C. L. Drum
Cardiovascular Research Institute
Department of Cardiology
1E Kent Ridge Road, 119228, Singapore
E-mail: mdccld@nus.edu.sg

G. Engudar, Prof. J. C. Y. Kah
Department of Biomedical Engineering
National University of Singapore
9 Engineering Drive 1, 117575, Singapore
E-mail: biekahj@nus.edu.sg

Dr. Y. Wang, Prof. B. Liedberg
Center for Biomimetic Sensor Science
School of Materials Science and Engineering
Nanyang Technological University
50 Nanyang Avenue, 639798, Singapore

Prof. T. Venkatesan
Department of Electrical Engineering
Department of Materials Science and Engineering
Department of Physics
National University of Singapore, 117581, Singapore

Prof. C. L. Drum
Translational Laboratory in Genetic Medicine
Agency for Science, Technology and Research (ASTAR)
8A Biomedical Grove, Immunos, Level 5, 138648, Singapore

1. Introduction

The "nano–bio" interface has been a domain of high interest in recent years. As nanoparticles (NPs) find increasing use in both diagnostic and therapeutic roles, the interface between engineered materials and complex human biology is experiencing an expanded focus due to its implications for nanomedicine and nanotoxicity.[1] Upon gaining access to the circulation, nanoparticles undergo an association with plasma components, forming a noncovalent protein corona around their surface. It is now known that this protein corona is dynamic in nature and that its identity changes over time.[2] The more abundant proteins bind to the exposed surface of the NP upon contact leading to a dynamic competition between the species already present on the surface and additional components which have slower association rates, but ultimately higher affinity for the surface.[3] It is also well understood that the chemical nature, charge, shape, and size of the NPs all play significant roles in the formation of the corona.[4]

The formation of the biomolecular corona plays an important role in the fate of the NP complex.[5] Hence, a platform to characterize the formation, evolution, and kinetics of corona on various nanomaterials becomes crucial for applications such as in vitro diagnostic sensors, in vivo diagnostic probes, or drug delivery technologies.[6] A commonly used method to study the protein corona formed around NPs is the enzymatic digestion of bound protein followed by polyacrylamide gel electrophoresis and/or mass spectroscopy.[7] While this method gives insight to the distribution of bound entities, it is not without limitations, i.e., taking significant manual effort with a large number of sequential experimental steps and typically 8–12 d[7a] for a complete workflow. Dynamic light scattering (DLS),[8] differential centrifugal sedimentation (DCS),[8,9] and size exclusion chromatography (SEC)[10] are additional, useful techniques that characterize the diffusional radius of nanoparticles and their bound coronas, however kinetic analyses are largely precluded due to technical limitations. As DLS is limited to colloidally stable NPs with a narrow size distribution (typically larger than 10 nm) and often has difficulty resolving unbound from bound corona components, fluorescence correlation spectroscopy (FCS)[11] has since emerged as an alternative to DLS, but it requires NPs to be first modified with a fluorescent tag.[12] The affinity of proteins for the NPs, however, may not be the same as their fluorescently labelled forms. Moreover, FCS is sensitive to the fluorescence of protein–NP complexes only if the autofluorescence from unbound proteins can be neglected. An additional drawback with DLS and FCS is their inability to provide meaningful data for anisotropic shapes.[7b] Furthermore, if the change in hydrodynamic radius of the protein–NP complex after adsorption is not significantly large, neither DLS nor FCS can feasibly resolve the change.[13] Hence the methods are usually used to investigate small NPs (but much larger than proteins themselves). There remains a need for a method which can return kinetic data from real-time interactions; be sufficiently adaptable to work for a variety of sizes, shapes, and chemical compositions and enable high-throughput data collection with high precision within reasonable time frames.

Surface plasmon resonance (SPR) is a technique that uses disruptions to surface plasmons, i.e., delocalized electrons on, typically, a gold surface, to study binding reactions with time resolved high fidelity measurements. Cedervall et al.[10] used SPR to observe dilute plasma modification of a biopolymeric NP, noting wide differences in disassociation rates as a function of hydrophobic content of the particle. A more recent study examined the effects of protein components on a SPR surface as they effected liposome absorption.[14] Although both studies demonstrated the utility of SPR in time-resolved NP recordings, neither study was able to report affinity constants or kinetic determinants of NP modification by individual plasma components.

In this study, we chose AuNPs as our model system because of their ease of synthesis, characterization, and relevance/use in targeted delivery applications. We immobilized native AuNPs on the surface without additional functionalization, thus enabling the study of serum proteins with the native surface of the AuNPs. Beyond studying the interactions of chosen serum proteins with native AuNPs, we used our protocol to study both polyethylene glycol (PEG) modification effects on blood components and hybrid targeted AuNPs interactions with serum.

To better understand the kinetic determinants of plasma component affinities to AuNPs, in addition to their relative adhesion efficiencies, we developed a multiplexed SPR assay using a commercially available (BioRad XPR36 SPR platform) reaction surface, thus enabling the extensive control measurements needed for subtraction of nonspecific and background binding. Through a layer-by-layer modification strategy, we could monitor the construction of modified AuNPs and then analyze them to obtain kinetic rate constants and relative adhesion amounts for specific plasma components, with experimental runs lasting no more than 3 h.

2. Results and Discussion

2.1. Immobilization of Gold NPs

The gold surface of the GLC chip from BioRad is supplied with a modified alginate polymer which provides a net negative charge and active sites for ligand immobilization. The alginate polymer layer also prevents nonspecific binding to the chip surface: a common artefact in SPR experiments. Sulfo-NHS (N-hydroxysulfosuccinimide) enables control and modification of carbodiimide crosslinking reactions involving activation of carboxylates (—COOH) for conjugation with primary amines (—NH$_2$). Derivatives are synthesized by mixing sulfo-NHS with a carboxyl-containing molecule and a dehydrating agent which in our case is 1-ethyl-3-(3-dimethylaminopropyl)carbodiimide (EDAC). Hence, the linker amino-EG6-undecanethiol hydrochloride is immobilized onto the chip through amide coupling. The corresponding change in SPR signal can be seen from time 0–600 s in the sensorgram showed in **Figure 1**A. The (—SH end of the linker is now free and the AuNPs are immobilized on the surface of the chip through these free (—SH groups. It is possible to monitor the immobilization in real time as seen from
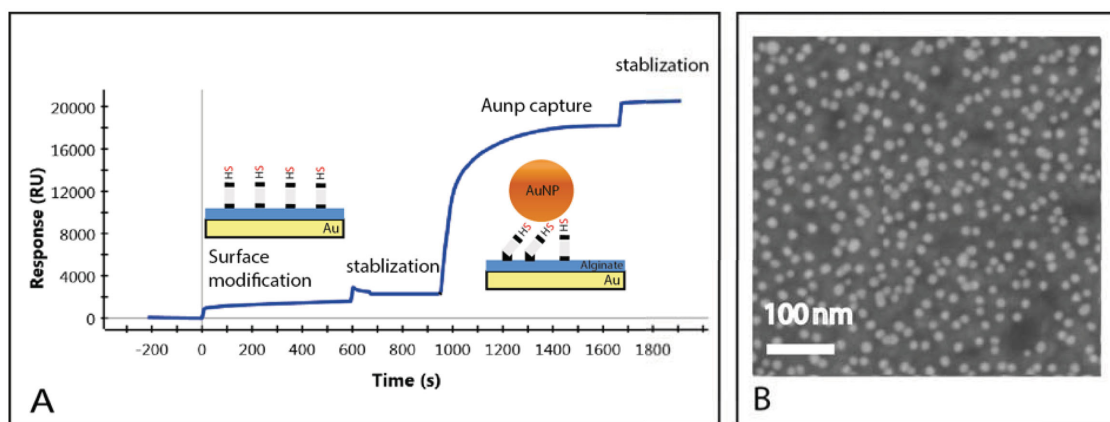
Figure 1. A) SPR sensorgram of surface modification using a hetero-bifunctional linker and subsequently, the immobilization of AuNPs. B) SEM image of the sensor surface after AuNP injection.

t = 950–1700 s in Figure 1A. The distribution and density of immobilized AuNPs was assessed directly using scanning electron microscopy (SEM) as seen in Figure 1B, allowing us to correlate SPR response with the final density of AuNP coating (refer Figure S1, Supporting Information). One advantage of being able to observe the systematic deposition and modification of nanoparticles in preparation of a downstream experiment is to ensure regularity of the substrate, i.e., differences in reactivity of linkage chemistries, particle formulations, and other formulations and other properties can be seen as aberrant profiles in the assembly stage, as visualized by real time SPR. Hence the method allows for step checks to enhance reproducibility across multiple runs. We would also like to highlight the platform nature of our protocol. By changing the linker molecule, it is potentially possible to immobilize additional classes of NP through diverse attachment chemistries and study its interactions, thereafter, with relevant proteins.

2.2. Studying Interactions of AuNPs with Proteins

One of the major advantages of multiplexing data acquisition using SPR is reproducibility. Owing to the availability of 6 × 6 microfluidic channels leading into 36 interaction spots that can be monitored simultaneously, it is possible to obtain 36 sensorgrams representing 36 interactions in a single experimental run. We designed our experiments to have unambiguous co-temporal controls to compare the experimental data to. These are set out in detail in the caption of **Figure 2** where a schematic representation has also been provided.

The four most common serum proteins found in nanoparticle coronas, human serum albumin (HSA), fibrinogen, immunoglobulin G (IgG), and apolipoprotein A1 (ApoA1), were selected for analysis.[15] After the AuNPs were immobilized and stabilized on the chip, three different concentrations of the four chosen proteins were flushed into the chip to observe the interactions. The association rate constant (i.e., k_{on} or on-rate), the dissociation rate constant (i.e., k_{off} or off-rate) and the equilibrium dissociation constant (K_D) were determined through first order kinetic curve fitting (**Table 1**).

The fibrinogen primary data are shown in Figure 2A–C. Sensorgrams for the three remaining proteins can be found in Figures S2–S4 (Supporting Information). The SPR surface has a very thin coating of alginate hydrogel to separate the gold surface from the tethered nanoparticle of interest. To demonstrate lack of interaction of the gold surface with the AuNPs, we employed a negative control lane wherein AuNP is flowed above the surface without activated linker chemistry. No interaction was observed in this setting. This is likely due to the separating effect of the thin layer of alginate hydrogel on the surface of the chip. Alginate typically forms a hydrogel with greater than 98% water content, creating a near native surface for AuNP attachment and minimizing surface adsorption (experiments with corona components and no AuNP also showed no interaction). Thus, although SPR has generally been an accepted methodology for component-specific kinetic studies of many types, there may exist differences with AuNPs experiencing full diffusional freedom, i.e., the corona kinetics of freely dissolved particles or colloidal suspensions.

ApoA1 has the lowest K_D of (0.12 ± 0.07) × 10^{-6} M, implying that it binds most strongly to the surface of the AuNP. Fibrinogen follows with a K_D of (0.53 ± 0.08) × 10^{-6} M. The affinity of HSA affinity for the surface of AuNP is about ten-fold lower than that of fibrinogen, bearing a K_D of (4.93 ± 2.41) × 10^{-6} M. IgG is the component with least affinity (amongst the four chosen serum components) bearing a K_D of (10.13 ± 3.28) × 10^{-6} M, implying it is about half as active as HSA with regard to adsorption onto the AuNP surface. Tsai et al.[16] have reported K_D values for interaction of bovine serum albumin (BSA) with AuNPs using Langmuir adsorption models on data obtained through electrospray-differential mobility analysis (1.96 × 10^{-6} M), fluorescence assay (1.61 × 10^{-6} M), and attenuated total reflectance Fourier transform infrared spectroscopy (0.6 × 10^{-6} M). As can be seen, the values of K_D for HSA-AuNP adsorption as obtained through SPR are within the same order of magnitude as BSA-AuNP adsorption, previously demonstrated through three different methods. To the best of our knowledge, kinetic and formal affinity constant data for the other major components interacting with AuNPs have not been previously reported.

We observed remarkable differences in k_{on} as obtained for the four proteins, while k_{off} values were comparable. ApoA1 (highest affinity) binds to the AuNP surface with an association constant almost 100 times higher than IgG
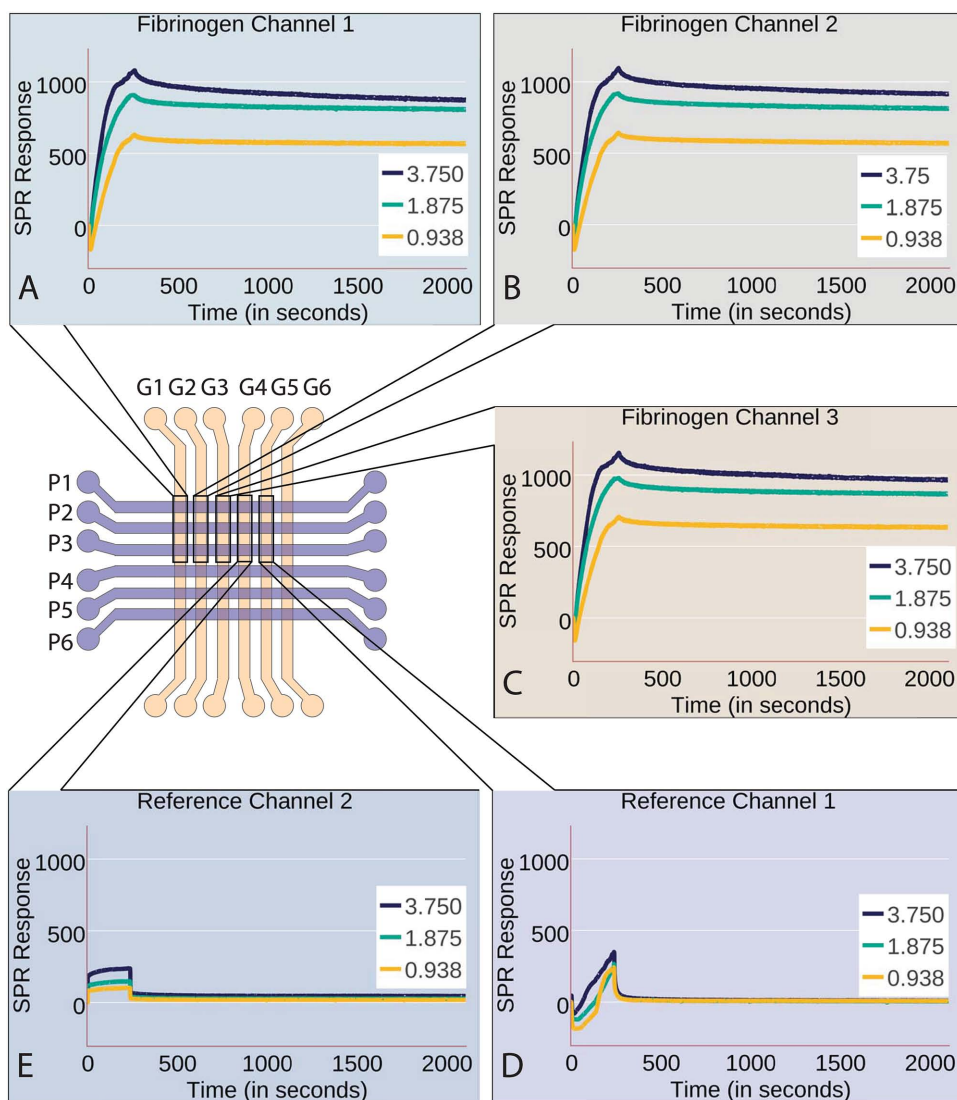
Figure 2. The microfluidic channel setup allowing multiplexed data collection is shown. AuNPs are immobilized in three channels G1, G2, and G3 using EDC/S-NHS coupling as described in methods. Two control channels (G4 and G5) are employed. G4 channel is modified with all the linker chemistry used to capture AuNPs (but AuNPs are not injected). G5 channel is in as received condition (alginate layer with inactive –COOH groups). Fibrinogen in three concentrations (3.750×10^{-6} M, 1.775×10^{-6} M, and 0.938×10^{-6} M) is injected along channels P1, P2, and P3 respectively. The three colored lines (blue, green, yellow) in each panel correspond to three different concentrations of fibrinogen used in the experiment (legend in white box in each panel). Sensorgrams A–C showing repeat measurements of three concentrations of fibrinogen with bare AuNPs available in channels G1, G2, and G3. D) Sensorgram resulting from the interaction of fibrinogen with the chemically active lane without the AuNPs. E) Sensorgram showing the interaction of fibrinogen with the unmodified surface (alginate polymer layer).

(lowest affinity). Overall, on-rates were found to play by far the largest role in the determination of component specific particle affinity for AuNPs.

Table 1. Kinetic rate constants and equilibrium dissociation constants for four chosen serum proteins as calculated from fitting curves to the experimentally obtained SPR responses.

Label	k_{on} [$M^{-1}\,s^{-1}$]	k_{off} [s^{-1}]	K_D [$\times 10^{-6}$ M]
HSA	466.860 ± 252.10	0.00184 ± 0.00033	04.93 ± 2.41
Fibrinogen	3857.330 ± 1031.08	0.00205 ± 0.00043	00.53 ± 0.08
IgG	232.47 ± 24.19	0.00233 ± 0.00068	10.13 ± 3.28
ApoA1	18634.00 ± 9590.50	0.00163 ± 0.00007	00.12 ± 0.07

Studies of absolute distributions of known plasma components are rare, the most relevant prior study may be of Mahmoudi et al.,[17] which described corona component binding to gold nanorods. This study used normalized spectral counts on LCMS (liquid chromatography mass spectrometry) to assign a relative binding amount of HSA and ApoA1 of 5.4 and 14.95, or a ratio of 1:2.8. Comparing values calculated using our kinetic measurements and known plasma concentrations of HSA and ApoA1, we arrive at a very similar ratio of 1:3 (Table S1, Supporting Information), consistent with the ability to approximate relative contributions to corona formation based on individualized kinetic and affinity measurements.

One significant limitation of the SPR approach is that component-specific kinetic data can only be extracted from

sensorgrams using purified reagents. In the setting of complex biofluids, serum, plasma, urine, etc., aggregate rates of modification can be observed, however measurement of component-specific rate constants in this setting is generally not possible.

There are also limitations to kinetic analysis as performed through SPR. Largely due to mass transport limitations, it is difficult to measure k_{on} values faster than about 10^6 M^{-1} s^{-1} accurately.[18] This upper limit is dependent on the size of the analyte. In case of analytes with high molecular mass, faster k_{on} values can be measured. This is because the larger signal produced by a large analyte allows the experiment to be performed at lower ligand densities, and lower ligand densities require lower rates of mass transport. For instance, a higher k_{on} of 10^7 M^{-1} s^{-1} was measured by SPR for the interaction between human immunodeficiency virus (HIV) Tat protein with integrin $\alpha_v\beta_3$.[19] In case of k_{off}, values slower than 10^{-5} s^{-1} can be difficult to accurately measure, mainly due to issues with instrument drift over long periods of time.[18,20]

2.3. Effect of PEGylation Observed through SPR

To evaluate the effect of PEG modification on plasma component binding, we used our multiplexed SPR protocol to establish saturating modification of thiolated PEG onto the AuNP based on the real-time SPR signal. Once surface saturation of PEG was achieved, we were able to demonstrate differential effects on plasma components and PEG

length-specific effects on NP modification by serum. Modification of injectable therapeutics with PEG is well known to affect circulation half-life and decrease protein binding.[21] However, more specific effects on individual plasma components is less clear. After immobilizing AuNPs on the chip surface, PEG-2000 was injected. To address the possibility that thiol groups on PEG-2000 may displace the immobilized AuNPs from the assay chip, we verified retention of the AuNPs through SEM images after the experiment was completed (Figure S1, Supporting Information). We observed that PEGylation was effective at preventing adhesion of all four serum proteins (**Figure 3**). The level of signal originating from adhesion of proteins was normalized to the level of signal change observed when the AuNPs were immobilized on the surface. It is seen that PEGylation is about 99% effective in blocking HSA (Figure 3A) while PEGylation is about 94% effective against fibrinogen (Figure 3B). The adsorption of IgG was reduced by about 93% (Figure 3C). PEGylation was found to be very effective against ApoA1 (Figure 3D) adsorption as well, showing a 98% decrease (Figure 3D).

It is important to note the significance of adsorption of proteins on NPs functionalized with antifouling agents (in this case PEG). Even though the amount of adsorption is small, if the adsorbing protein triggers cell surface receptors, the uptake machinery of the cell may be activated. In turn, this would lead to internalization of the NP by the reticuloendothelial system (RES) and thereby reduce circulation time. Further, the adsorption of other complement proteins such as C1q, MBL, ficolin, and C3b, even at trace amount, would be sufficient to trigger an undesirable complement activation.
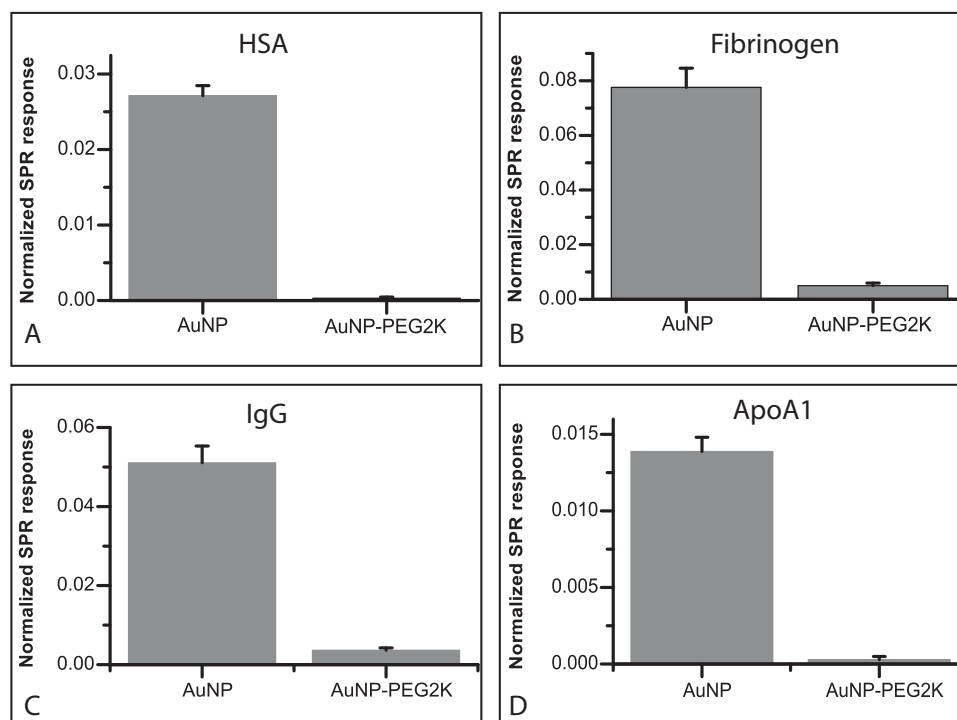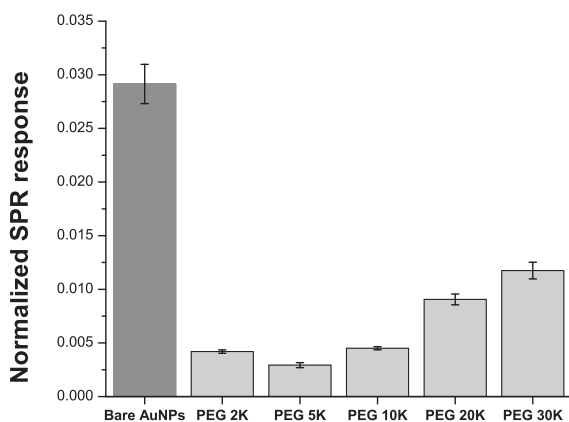

Figure 3. Normalized SPR response for interaction of individual serum proteins with AuNPs modified with PEG 2k compared to unmodified AuNPs. The absolute response obtained due to adsorption of proteins to modified and unmodified AuNPs is divided by the absolute response caused by the immobilization of AuNPs on the sensor surface. This normalization, hence, takes care of the minor differences in number of AuNPs captured in each lane. Compared to unmodified AuNPs, all sets of data from serum proteins were significantly different (p-value << 0.05).

2.4. Effect of Varying PEG Chain Length on Resistance to Corona

After having validated the effect of PEGylation on individual plasma components, we decided to investigate the effect of PEG chain length moieties on the resistance of the functionalized NP to corona formation. To accomplish this study, PEG molecules having average molecular weights (M_Ws) of 2k, 5k, 10k, 20k, and 30k were chosen. After duly immobilizing AuNPs on the chip surface as before, we injected the chosen PEG moieties, each in a separate lane, leaving a control lane with unmodified AuNPs. This lane would serve as a control to compare our findings to. All absolute responses were normalized to the SPR response resulting from the capture of AuNPs in the designated lanes, to allow for cross comparability.

The nanomedicine community has long been dealing with the "PEG dilemma."[22] Due to the presence of its long apolar chains, PEG has been shown to reduce protein adsorption. However in recent years, PEGylation has also been shown to strongly inhibit cellular uptake and limit the binding with intended protein targets thereby reducing the potential of drug delivery significantly. Hence, the emerging trend seems to revolve around optimization – such that the functionalization is made to retard protein adsorption but not so much that it limits its ability to be trafficked into cells and deliver its cargo.

Here, we found that PEG 2k, PEG 5k, and PEG 10k are very similar in their resistance to corona formation allowing only 14%, 10%, and 15% adsorption, respectively, as compared with an unmodified surface (**Figure 4**). PEG 20k and 30k were the least effective antifouling moieties of the group allowing 31% and 40%, respectively. Hence PEG 2k, 5k, and 10k are about—three to four times more effective than the longer chained ones. Our data is thus consistent with prior reports indicating that shorter PEG chains pack more tightly to the surface of an exposed NP thereby creating a more efficient shield against nonspecific protein adsorption on the surface.[23]

As the PEG chain length increases, the PEG molecules are understood to adopt a "mushroom" conformation with reduced packing density that allow proteins to bind to available exposed areas on the NP surface.[24] It has been previously suggested that protein adsorption to PEG grafted surfaces is very sensitive to chain density effects and less so to chain length.[23,25] Although our data are consistent with this hypothesis, further experiments will need to be performed to accurately characterize steric effects of linear and branched PEG molecules. Likewise, there are conflicting reports in literature regarding the effect of the chain length on adsorption. Gref et al.[26] have reported that when polylactic acid (PLA) NPs were functionalized with varying lengths of PEG, the most amount of protein is found adsorbed to PEG 2k, PEG 5k, 10k, 15k, and 20k are all similar in their resistance to adsorption and they adsorb about 40% of protein that is adsorbed by PEG 2k. On the other hand, a more recent report by Pozzi et al.[27] claims that when varying chain lengths of PEG are used to functionalize multicomponent cationic liposomes, PEG 1k adsorbs the most amount of proteins while PEG 2k and PEG 5k both adsorb about 50% of PEG 1k.

2.5. Observation of Hybrid Modifications Effect on NP Targeting Design

NP technologies engineered for therapeutic applications are often multifunctional, containing materials that target to the site of disease, optimize plasma half-life, and provide therapeutic or imaging modalities. When the complexity of NP design is tested in vivo, interactions beyond the four major plasma components may become important. In particular, for particles that are functionalized with a specific targeting moiety, the cumulative effects of antifouling modifications may relate directly to binding capacity. Consequently, we synthesized a model NP system (named "hybrid" in **Figure 5**) to have a corona retarding moiety – the commonly used SH-PEG 2k and a target binding moiety –SH-PEG 5k-biotin (the target being streptavidin). The two controls that were used in this experiment were AuNPs functionalized with only SH-PEG 2k and AuNPs functionalized with only SH-PEG 5k-biotin (referred to as biotin). It is logical to conclude, in the hybrid configuration, the biotin end of the –SH-PEG 5k-biotin molecule will be accessible above the packing layer of –SH-PEG 2k (since PEG 5k is longer than PEG 2k). Figure 5A shows the sensorgram from the interaction of 20% human serum with the functionalized AuNPs. The inset shows the schematic illustration of the interaction. To be able to compare the performance of the NP systems with respect to its resistance to biomolecular fouling and its ability to bind its intended target streptavidin, on each type of NP system, we have normalized the absolute SPR responses resulting from serum interaction and streptavidin binding to the level of gold initially captured in the lane. Compared to unmodified AuNP, all the lanes showed a drastic drop. PEG is well known to resist protein adsorption and hence the surface of the AuNP functionalized with PEG 2k shows 18% of the adsorption signal observed in the bare gold surface AuNPs. Likewise, PEG linked biotin shows
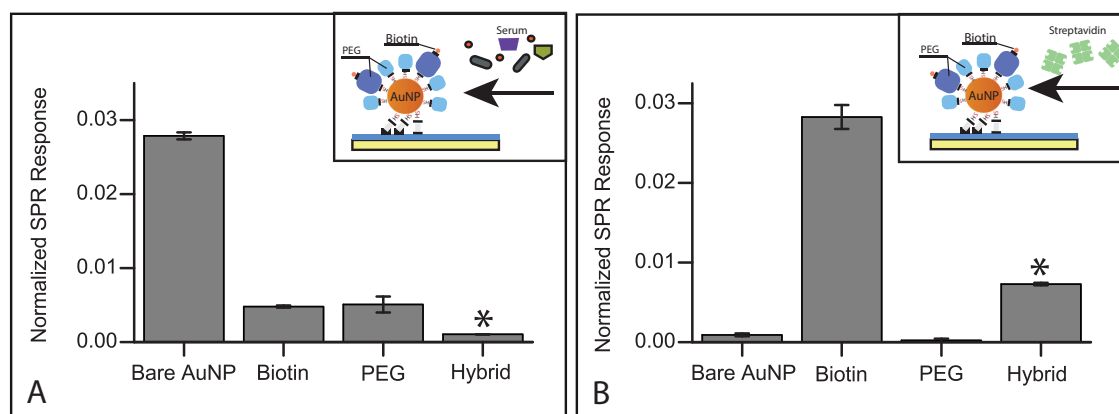
Figure 4. Normalized SPR response for interaction of 20% (w/v) human serum (diluted with PBS buffer) with AuNPs modified with PEG 2k, PEG 5k, PEG 10k, PEG 20k, and PEG 30k compared to unmodified AuNPs. With the exception of PEG 2k and PEG 5k, all sets of data were statistically different from all other sets (p-value << 0.05).

Figure 5. A) Normalized SPR response for interaction of 20% human serum with AuNPs modified with PEG 5k-biotin (referred to as "biotin"), PEG 2k, and 1:1 mixture of biotin:PEG 2k (referred to as "hybrid") compared to unmodified AuNPs. The inset illustrates the schematic of the experiment. B) Normalized SPR response showing the ability of AuNPs with previously described functionalizations to bind intended target streptavidin. The inset illustrates the schematic of the experiment. Statistically significant results have been marked with a (*) mark (p-value << 0.05).

about 17% adsorption when compared with unfunctionalized surface. The hybrid system, dramatically, shows only 3% adsorption of when compared with bare AuNP. We hypothesize this might be caused by a favorable interplay between the shielding accorded by the PEG 2k moiety and the PEG 5k section of the PEG 5k-biotin moiety. The exact affinity of this hybrid system for serum proteins may perhaps be tailored by playing upon the ratio between SH-PEG and SH-PEG-biotin moieties.

In NP formulations, addition of new components almost always involves a trade-off with other functionalities. We thus studied the trade-off of biotin streptavidin binding in the setting of additional PEG modification, in the highly controlled setting of multiplexed SPR. Figure 5B shows the sensorgram for the interaction of streptavidin with these modified AuNPs (schematic in inset). As expected, the unmodified AuNP showed almost no nonspecific adsorption of streptavidin (3%). The AuNP with PEG alone showed no response because there was no biotin present. However, when we examined the biotin and hybrid systems, we were able to determine the precise trade-off in terms of streptavidin binding with 26% of streptavidin bound when compared with the original biotin-only particle. That the interaction is truly between biotin–streptavidin is evident from the extremely low off-rate and lack of interaction seen in control lanes. It should also be stated that since the surface of the AuNP in the case of the hybrid is shared by –SH-PEG 2k and –SH-PEG 5k-biotin, the number of available biotin groups for binding streptavidin will be much lesser than the case where the AuNP is modified with –SH-PEG 5k-biotin alone. Hence a part of the reduced response can be attributed to a lesser number of target-binding ligands.

3. Conclusion

We have established a robust protocol which can be used to study interactions of NPs with biomolecular entities of interest. Using multiplexed SPR measurements, including extensive controls, we were able to accurately determine kinetic measurements of plasma component interactions with AuNPs, including wide variation in association constants for individual plasma components, and conduct comparative studies of corona formation. In principle, the same protocol could be applied to a wide variety of NP materials and formulations as only a single point of attachment is required for the SPR surface and many NPs lie within the theoretical plasmonic sensing range of 100 nm. Although, in principle, the techniques and analysis of tethered polymeric NPs should be very similar to the AuNPs in this study, key differences in operational efficiency will be known only upon additional experimentation. Because test-particles are assembled on-chip, the ability to show saturation kinetics helps to ensure stabilized surface occupancy of modifying agents. The ability to perform multiple assays alongside proper controls using the same reagents on the same chip is of particular value given the multicomponent nature of nanoparticle designs and demonstrates the strength of multiplexed SPR.

4. Experimental Section

4.1. Synthesis of AuNPs

The NPs were synthesized using the method of Frens et al.[28] 100 mL of 1×10^{-3} M hydrochloroauric acid (HAuCl$_4$) was heated until it boiled. 15 mL of 38.8×10^{-3} M trisodium citrate was added to the solution while being vigorously stirred. After being boiled for 15 min, the solution changed color from pale yellow to purple before finally becoming a deep red NP colloid. The citrate-capped NP colloid was washed twice through centrifugation at 10 000 rpm for 15 min and diluted ten fold for subsequent experiments. The zeta potential and hydrodynamic diameter (DH) of the NPs were measured at 25 °C using a DLS (Nano ZS, Malvern, UK), and the morphology characterized using transmission electron microscopy (TEM) (JEM-1220, JEOL Ltd., Japan). The concentration of the NPs was determined by optical absorption. The synthesized NPs were stored at 4 °C until further experiments.

4.2. Immobilization of AuNPs onto the Chip Surface

A Bio-Rad ProteOn XPR36 instrument (Haifa, Israel) was used in this study. The GLC-type sensor chip consists of a glass prism coated with gold and an alginate layer with a low capacity for ligand conjugation. A detailed introduction of experimental protocol for ligand-analyte interactions can be found in literature.[29] The system was first equilibrated with phosphate buffered saline-tween (PBS-T) buffer (20×10^{-3} M Na-phosphate, 150×10^{-3} M NaCl, and 0.05% Tween 20, pH 7.4). The channels of the chip were activated for 5 min with a mixture of EDAC (0.2 M) and sulfo-NHS (0.05 M), followed by 10 min injection of 1×10^{-3} M amino-EG6-undecanethiol (Dojindo Laboratories, Japan) and 5 min injection of ethanolamine-HCl solution. Subsequently, AuNPs were injected onto the modified sensor lane for 6 min with a flow rate of 30 μL min^{-1}. The chip is then flushed PBS-T for 30 min to monitor the dissociation of AuNP from the surface.

4.3. Studying Interactions of Serum Components with Immobilized AuNPs

Using aforementioned methods, 17 nm AuNPs were captured on the SPR chip surface and stabilized for 30 mins. HSA, human fibrinogen, human immunoglobulin G (IgG), and human apolipoprotein A1 (ApoA1) were dissolved in PBS and injected into the AuNP modified sensor surface. The injection time was 4 min at a flow rate of 100 μL min^{-1}, followed by a dissociation step of 30 mins. It has to be noted that the direction of injection of the proteins is orthogonal to the direction in which the AuNPs are injected. Please refer to Figure 2 for the layout of the chip. This means that in a single protein lane, we can obtain interaction sensorgrams ($1 \leq n \leq 6$, depending on how many lanes have been populated with AuNPs).

4.4. Curve Fitting to Evaluate Kinetic Parameters

The data obtained from the experiments were exported to and analyzed with Origin software package For the dissociation phase

$$R_d = R_{d0} + A_1 e^{-k_{off}t} \tag{1}$$

where R_d is the response at any time t in the dissociation phase, R_{d0} is the response at the start of the as chosen dissociation phase, A is a constant, k_{off} is dissociation constant, and t is time in seconds. In the association phase

$$R_a = A_2 - A_3 e^{-kt} \tag{2}$$

where R_a is the response at any time in the association phase, A_2 and A_3 are constants and t is time in seconds. The parameter k will be used to determine k_{on}, by the formula given below

$$k_{on}C + k_{off} = k \tag{3}$$

where k_{off} is dissociation constant calculated from Equation (1), k is the parameter obtained from Equation (2), and C is concentration of protein in moles L^{-1}. Finally

$$K_D = \frac{k_{off}}{k_{on}} \tag{4}$$

While fitting curves, care has to be taken to select such portions of the responses which are free from bulk refractive index changes. An example has been provided in Figure S5 (Supporting Information).

4.5. Studying Interactions of Serum Components with PEGylated AuNPs

The 17 nm AuNPs were captured on the SPR chip surface (as described above) and stabilized for 30 min. Thiolated PEG 2k (Lysanbio, AL, USA) was dissolved in water to a concentration of 100×10^{-3} M and was injected onto the AuNPs modified SPR sensor surface. The injection time was 2 min followed by a stabilization step of 10 min. For protein injection, all four chosen serum components HSA, fibrinogen, IgG, and ApoA1 were dissolved in PBS, as in the previous section. Then the sensor chip was rotated by 90° and the four proteins were injected on to the sensor surface at a flow rate of 100 μL min^{-1}.

4.6. Studying Effect of PEG Chain Length on Corona Formation

The 17 nm AuNPs were captured on the SPR chip surface (as described above) and stabilized for 30 mins. Thiolated PEG 2k, PEG 5k, PEG 10k, PEG 20k, and PEG 30k (Lysanbio, AL, USA) were dissolved in water, each separately, to a concentration of 100×10^{-3} M each and were injected onto the AuNPs modified SPR sensor surface. The injection time was 2 min followed by a stabilization step of 10 min 20% diluted human serum was injected after the chip was rotated through 90°. The interaction between serum and PEGylated AuNPs was made to occur for 2 min after which the injection of serum was stopped and lanes were flushed with PBS-T buffer to observe the dissociation phase.

4.7. Studying the Interaction of Serum and Streptavidin with Model Hybrid NP Systems

In this experiment, we first make the following solutions: (a) 200×10^{-6} M of SH-PEG-biotin (M_W 5k), denoted as "biotin" in Figure 5, (b) 200×10^{-6} M of SH-PEG-biotin (M_W 5k), and 100×10^{-6} M SH-PEG (M_W 2k), denoted as hybrid in Figure 5, (c) 100×10^{-6} M of SH-PEG (M_W 2k), denoted as PEG in Figure 5.

Using previously mentioned methods, 17 nm AuNPs were captured on the SPR chip surface and stabilized for 30 mins. A hybrid layer of surface functionalization material is formed on the AuNPs by co-injection of 100×10^{-6} M of thiolated PEG 2k (Lysanbio, US) and 200×10^{-6} M of thiolated PEG-biotin (Thermos Scientific), both dissolved in water. Using the same protocol, two other lanes were modified using 100×10^{-6} M of thiolated PEG 2k and 200×10^{-6} M of thiolated PEG-biotin, respectively. Human serum (Sigma-Aldrich, MO, USA) was diluted to 20% using PBS and injected onto the SPR sensor. Streptavidin (Sigma-Aldrich, MO, USA) was dissolved in PBS buffer and injected onto the SPR sensor at a concentration of 100×10^{-6} M. The injection times for both analytes were 2 min at a

flow rate of 100 µL min^{-1} and sensor responses were recorded at 100 s after injection period. The sensor's interspots, which are the native surface of the sensor, were used as reference and all signals were subtracted from the reference signal.

[1] a) S. H. Brewer, W. R. Glomm, M. C. Johnson, M. K. Knag, S. Franzen, *Langmuir* **2005**, *21*, 9303; b) D. M. Brown, C. Dickson, P. Duncan, F. Al-Attili, V. Stone, *Nanotechnology* **2010**, *21*, 215104; c) A. Bajaj, B. Samanta, H. Yan, D. J. Jerry, V. M. Rotello, *J. Mater. Chem.* **2009**, *19*, 6328; d) D. Boraschi, L. Costantino, P. Italiani, *Nanomedicine* **2011**, *7*, 121; e) T. Cedervall, *Proc. Natl. Acad. Sci. USA* **2007**, *104*, 2050; f) B. Fadeel, A. E. Garcia-Bennett, *Adv. Drug Deliv. Rev.* **2010**, *62*, 362.

[2] a) E. Casals, T. Pfaller, A. Duschl, G. J. Oostingh, V. Puntes, *ACS Nano* **2010**, *4*, 3623; b) D. Dell'Orco, M. Lundqvist, C. Oslakovic, T. Cedervall, S. Linse, *PLoS ONE* **2010**, *5*, e10949.

[3] a) M. Gasser, *J. Nanobiotechnol.* **2010**, *8*, 31; b) A. Cifuentes-Rius, H. de Puig, J. C. Y. Kah, S. Borros, K. Hamad-Schifferli, *ACS Nano* **2013**, *7*, 10066.

[4] a) Z. J. Deng, *Nanotechnology* **2009**, *20*, 455101; b) J. C. Y. Kah, C. Grabinski, E. Untener, C. Garrett, J. Chen, D. Zhu, S. M. Hussain, K. Hamad-Schifferli, *ACS Nano* **2014**, *8*, 4608.

[5] a) J. V. Georgieva, *Mol. Ther.* **2011**, *19*, 318; b) P. Ghosh, *J. Am. Chem. Soc.* **2010**, *132*, 2642; c) S. Tenzer, D. Docter, J. Kuharev, A. Musyanovych, V. Fetz, R. Hecht, F. Schlenk, D. Fischer, K. Kiouptsi, C. Reinhardt, *Nat. Nanotechnol.* **2013**, *8*, 772.

[6] T. G. Iversen, T. Skotland, K. Sandvig, *Nano Today* **2011**, *6*, 176.

[7] a) D. Docter, U. Distler, W. Storck, J. Kuharev, D. Wünsch, A. Hahlbrock, S. K. Knauer, S. Tenzer, R. H. Stauber, *Nat. Protocols* **2014**, *9*, 2030; b) M. Mahmoudi, A. M. Abdelmonem, S. Behzadi, J. H. Clement, S. Dutz, M. R. Ejtehadi, R. Hartmann, K. Kantner, U. Linne, P. Maffre, S. Metzler, M. K. Moghadam, C. Pfeiffer, M. Rezaei, P. Ruiz-Lozano, V. Serpooshan, M. A. Shokrgozar, G. U. Nienhaus, W. J. Parak, *ACS Nano* **2013**, *7*, 6555; c) A. Jedlovszky-Hajdú, F. B. Bombelli, M. P. Monopoli, E. Tombácz,

K. A. Dawson, *Langmuir* **2012**, *28*, 14983; d) A. Lesniak, F. Fenaroli, M. P. Monopoli, C. Åberg, K. A. Dawson, A. Salvati, *ACS Nano* **2012**, *6*, 5845; e) S. Tenzer, D. Docter, S. Rosfa, A. Wlodarski, J. Kuharev, A. Rekik, S. K. Knauer, C. Bantz, T. Nawroth, C. Bier, J. Sirirattanapan, W. Mann, L. Treuel, R. Zellner, M. Maskos, H. Schild, R. H. Stauber, *ACS Nano* **2011**, *5*, 7155.

[8] M. P. Monopoli, D. Walczyk, A. Campbell, G. Elia, I. Lynch, F. B. Bombelli, K. A. Dawson, *J. Am. Chem. Soc.* **2011**, *133*, 2525.

[9] D. Walczyk, F. B. Bombelli, M. P. Monopoli, I. Lynch, K. A. Dawson, *J. Am. Chem. Soc.* **2010**, *132*, 5761.

[10] T. Cedervall, I. Lynch, S. Lindman, T. Berggård, E. Thulin, H. Nilsson, K. A. Dawson, S. Linse, *Proc. Natl. Acad. Sci.* **2007**, *104*, 2050.

[11] a) T. Liedl, S. Keller, F. C. Simmel, J. O. Rädler, W. J. Parak, *Small* **2005**, *1*, 997; b) G. U. Nienhaus, P. Maffre, K. Nienhaus, in *Methods in Enzymology*, Vol. *519* (Ed: Y. T. Sergey), Academic Press, San Diego, CA, USA **2013**, pp. 115–137.

[12] F. Zhang, E. Lees, F. Amin, P. R. Gil, F. Yang, P. Mulvaney, W. J. Parak, *Small* **2011**, *7*, 3113.

[13] E. J. Cho, H. Holback, K. C. Liu, S. A. Abouelmagd, J. Park, Y. Yeo, *Mol. Pharm.* **2013**, *10*, 2093.

[14] M. Canovi, J. Lucchetti, M. Stravalaci, F. Re, D. Moscatelli, P. Bigini, M. Salmona, M. Gobbi, *Sensors* **2012**, *12*, 16420.

[15] a) P. Aggarwal, J. B. Hall, C. B. McLeland, M. A. Dobrovolskaia, S. E. McNeil, *Adv. Drug Deliv. Rev.* **2009**, *61*, 428; b) P. P. Karmali, D. Simberg, *Exp. Opin. Drug Deliv.* **2011**, *8*, 343; c) T. Göppert, R. Müller, *Int. J. Pharm.* **2005**, *302*, 172.

[16] D.-H. Tsai, F. W. DelRio, A. M. Keene, K. M. Tyner, R. I. MacCuspie, T. J. Cho, M. R. Zachariah, V. A. Hackley, *Langmuir* **2011**, *27*, 2464.

[17] M. Mahmoudi, S. E. Lohse, C. J. Murphy, A. Fathizadeh, A. Montazeri, K. S. Suslick, *Nano Lett.* **2013**, *14*, 6.

[18] S. Núñez, J. Venhorst, C. G. Kruse, *Drug Discovery Today* **2012**, *17*, 10.

[19] C. Urbinati, A. Bugatti, M. Giacca, D. Schlaepfer, M. Presta, M. Rusnati, *J. Cell Sci.* **2005**, *118*, 3949.

[20] R. Chu, D. Reczek, W. Brondyk, *Sci. Rep.* **2014**, *4*, 7360.

[21] a) H. Otsuka, Y. Nagasaki, K. Kataoka, *Adv. Drug Deliv. Rev.* **2003**, *55*, 403; b) H. R. Kim, *Electrophoresis* **2007**, *28*, 2252.

[22] H. Hatakeyama, H. Akita, H. Harashima, *Biol. Pharm. Bull.* **2013**, *36*, 892.

[23] S. I. Jeon, J. H. Lee, J. D. Andrade, P. G. De Gennes, *J. Coll. Interface Sci.* **1991**, *142*, 149.

[24] J. C. Y. Kah, K. Y. Wong, K. G. Neoh, J. H. Song, J. W. P. Fu, S. Mhaisalkar, M. Olivo, C. J. R. Sheppard, *J. Drug Target.* **2009**, *17*, 181.

[25] T. McPherson, A. Kidane, I. Szleifer, K. Park, *Langmuir* **1998**, *14*, 176.

[26] R. Gref, M. Lück, P. Quellec, M. Marchand, E. Dellacherie, S. Harnisch, T. Blunk, R. H. Müller, *Coll. Surf. B* **2000**, *18*, 301.

[27] D. Pozzi, V. Colapicchioni, G. Caracciolo, S. Piovesana, A. L. Capriotti, S. Palchetti, S. De Grossi, A. Riccioli, H. Amenitsch, A. Lagana, *Nanoscale* **2014**, *6*, 2782.

[28] G. Frens, *Nature* **1972**, 20.

[29] O. Nahshol, V. Bronner, A. Notcovich, L. Rubrecht, D. Laune, T. Bravman, *Anal. Biochem.* **2008**, *383*, 52.